Journal of Non-Newtonian Fluid Mechanics 193 (2013) 103–115

Contents lists available at SciVerse ScienceDirect

Journal of Non-Newtonian Fluid Mechanics

journal homepage: http://www.elsevier.com/locate/jnnfm

Squeeze flow of semi-solid slurries

Andreas N. Alexandrou [a], Georgios C. Florides [a], Georgios C. Georgiou [b,*]

[a] Department of Mechanical and Manufacturing Engineering, University of Cyprus, P.O. Box 20537, 1678 Nicosia, Cyprus
[b] Department of Mathematics and Statistics, University of Cyprus, P.O. Box 20537, 1678 Nicosia, Cyprus

ARTICLE INFO

Article history:
Available online 5 October 2012

Keywords:
Squeeze flow
Bingham model
Thixotropy
Structural parameter
Computational rheology
Finite elements

ABSTRACT

A standard method used to determine material properties of semi-solid slurries is the squeeze flow experiment; a fixed amount of material is squeezed under constant force or velocity and the relation between the force and the displacement of the sample provides information about the rheology of the slurry. The objective of this work is to contribute to the further development of the squeeze flow methodology in order to accurately determine material properties. This is achieved by a model that accounts for the finite yield stress and the thixotropy of the slurry. More specifically a structural viscoplastic model based on the Bingham plastic constitutive equation is proposed. The yield stress is assumed to vary linearly with the structural parameter which follows a first-order rate equation accounting for the material structure break-down and build-up. Numerical experiments of squeeze flow under either constant load or constant velocity are presented and discussed. Comparisons with their non-thixotropic counterparts are made in the case of compression under constant load. The development of the yielded/unyielded regions in relation to material structural changes is analyzed. The numerical results show that initially thixotropy does not affect the flow. However, once the structure is destroyed, the unyielded regions grow slower than the non-thixotropic case allowing for longer compression of the sample. Under constant force the structure may be destroyed at the early stages of the compression but at a later time it re-builds steadily till the cessation of the flow experiment. Under constant velocity, however, the structure is destroyed steadily. Depending then on the case, the final internal structure of the squeezed material can vary significantly. This is an important issue that needs to be taken into consideration in the evaluation of the material parameters.

1. Introduction

The motivation of the present work comes from our interest in the processing of semi-solid slurries. These are relatively dense suspensions of specially prepared spheroidal particles, known to be viscoplastic, i.e. they flow only if a finite stress value is exceeded; otherwise, they behave as solids [1,2]. The viscoplastic behavior of semi-solid slurries is due to particle welding, dry friction, and hydrodynamic forces. Semi-solid slurries also exhibit thixotropic behavior, i.e. their viscosity decreases with time under constant shearing [3,4]. However, in contrast to other thixotropic materials, the rheological properties of semi-solid slurries are partially reversible [5,6]. Other materials exhibiting similar behavior are greases, waxy crude oils, and fermentation broths [7]. Understanding the influence of thixotropy on the flow behavior and the structural evolution of these materials during flow is of great importance to the industry.

An early review on thixotropy is that of Mewis [8], who discussed the various experimental techniques for detecting and evaluating thixotropy in real materials. Later, Barnes [9] discussed typical experimental methods for measuring thixotropy and the related mathematical theories. He also pointed out the need of developing more accurate models to describe the microstructure evolution, taking into account the time dependence of viscosity. The concept of thixotropy and its various rheological manifestations with focus on particular suspensions have been recently reviewed by Mewis and Wagner [7], who pointed out that a general rheological model, capable to describe its different features, has not yet been developed. Useful discussions of the thixotropy literature were also provided by Mujumdar et al. [10] and de Souza Mendes [11].

Mewis and Wagner [7] categorized thixotropic models into three classes: the phenomenological models, which are based on the general principles of rational continuous mechanics, the models that use an internal or "structure" parameter to describe the material structure, and those that are based on a microstructure approach. The first two classes can generate both inelastic and viscoplastic equations of state and form a continuous spectrum of models. Phenomenological models include those incorporating a memory function based on continuum mechanics principles and those that employ a structure parameter. In the latter models

* Corresponding author. Tel.: +357 22892612; fax: +357 22892601.
E-mail address: georgios@ucy.ac.cy (G.C. Georgiou).

0377-0257/$ - see front matter © 2012 Elsevier B.V. All rights reserved.
http://dx.doi.org/10.1016/j.jnnfm.2012.09.007

the rheological response is associated to the instantaneous structure, which is governed by the kinetic equation for structure parameter. As noted by Mewis and Wagner [7], structural parameter models can be viewed as extremely simplified microstructural models. On the other hand, such simple models are more general and may be applied to a wider class of materials.

In a recent work, Alexandrou and Georgiou [12] introduced a modified Herschel–Bulkley model that included a structural parameter and applied a novel computational method suitable for moving free-boundary problems to study the flow of a thixotropic semi-solid material between two coaxial cylinders. The strength of the slurry or the yield stress, which is attributed to welded bonds, dry friction, and hydrodynamic forces, was assumed to be a function of the structural parameter. The same authors subsequently employed a similar structural model to simulate the flow of a thixotropic shear thinning material (e.g. semi-solid suspension) in a concentric cylindrical rheometer and investigated the effects of shear rejuvenation, aging and shear banding phenomena [3]. Their numerical simulations were found to be in agreement with certain experimental data of Beris et al. [13] for concentrated star polymer suspensions and demonstrated that the rate of breakdown and build-up equilibrium is reached in shorter times for fluids with large build-up coefficients, which may be important in shearing applications. It was also noted that the time scales needed for the shear banding to develop are similar to those found in semi-solid processes [3].

Structural thixotropy models for semi-solid materials have also been employed by Gautham and Kapur [14] and by Koeune and Ponthot [15]. The former authors proposed a model for unsteady state shear stress of semi-solid suspensions with a structural parameter representing the degree of connectivity or aggregation in the fluid. This model focuses on the fast transient stage of the process, simulates the structure build-up in the absence of applied shear, and computes the steady state structure for a given shearing rate after long shearing time. It was found that, depending on the initial conditions of the structure (time, temperature, shear cycle, etc.), the build-up increases rapidly in the beginning and thereafter more slowly, eventually reaching the maximum value of a fully-structured material. Koeune and Ponthot [15] proposed a thermo-mechanical model for semi-solid thixoforming to describe the proper degeneration to pure solid or liquid as well as free solid suspension behavior. They considered as an internal material parameter the effective liquid fraction, which excludes the entrapped liquid inside the solid grains and does not contribute to the flow. The proper degeneration of the suspension to pure solid and pure liquid as well as to free solid suspension aims to overcome the limitations of their previous model of semi-solid thixoforming.

A microstructural model has been proposed by Favier and Atkinson [4] who analyzed the transient behavior of concentrated semi-solid materials in rapid compression test simulations. Their model is based on micromechanical and homogenization techniques, which assumes that semi-solids exhibit elastic–viscoelastic response under rapid compression. It was shown that the experimental load–displacement curve initially increases up to maximum and thereafter decreases and increases again. They also found that the effect of solid fraction on mechanical response is in qualitative agreement with experiments.

The objectives of the present work are: (a) to investigate numerically the structural changes of a thixotropic yield-stress material in squeeze flow, and (b) to contribute to the use of squeeze flow for the rheological characterization of semi-solid slurries. To that end, we employ a thixotropic model based on the Bingham plastic constitutive equation with the yield stress depending linearly on a structural parameter [3,12]. This can be viewed as an extension of our previous work, where the flow and shape evolution during the squeeze flow of a finite amount of a non-thixotropic Bingham plastic were investigated by means of numerical simulations [16].

It should be noted that while the motivation and most of the literature reviewed above concern the behavior of semi-solid slurries, the theory and the model presented below apply to a much larger family of materials. The importance of considering thixotropy in flow analysis of viscometric flows has been recently emphasized by Potanin [17] and Ardakani et al. [18]. Early theoretical analyses and numerical studies of the squeeze flow of viscoplastic materials have been reviewed by Smyrnaios and Tsamopoulos [19]. Engmann et al. [20] also presented a comprehensive review of squeeze flow theory and its applications to rheometry for a wide class of materials, including generalized Newtonian, yield-stress, and viscoelastic fluids, and provided a long list of useful references. Additional references may be found in [21] and in the recent paper of Shaukat et al. [22].

In Section 2, the thixotropy model as well as the governing equations and boundary and initial conditions for the squeeze flow experiment are presented. The sample is compressed on the top either under constant load or constant velocity while its bottom side is fixed. In Section 3, the numerical method is briefly discussed. In Section 4, the numerical results are presented and the evolution of the structural parameter in the sample, which is important in understanding the structural and rheological changes during flow, is discussed. Two-dimensional (time-dependent) results for the distribution of the structural parameter in the sample are presented for the first time and compared with the corresponding evolution of the yielded and unyielded regions. Finally, concluding remarks are provided in Section 5.

2. Governing equations

It is assumed that a cylindrical sample of the material, of initial radius R_0 and height H_0, is placed between two parallel discs (Fig. 1) and is then compressed from the top under constant load or constant velocity and isothermal conditions, while the lower disc remains fixed. In incompressible flow under zero gravity, the continuity and momentum equations for any fluid become:

$$\nabla \cdot \underline{u} = 0 \tag{1}$$

and

$$\rho \frac{D\underline{u}}{Dt} = -\nabla p + \nabla \cdot \underline{\tau} \tag{2}$$

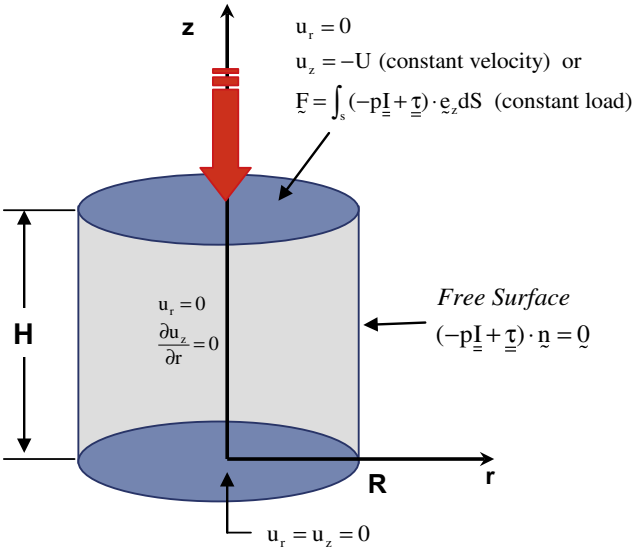

Fig. 1. Geometry and boundary conditions of the squeeze flow experiment. At $t = 0$ the sample is at rest.

where $\underline{u}$ is the velocity vector, p is the pressure, $\underline{\underline{\tau}}$ is the viscous stress tensor, t is the time, $D\underline{u}/Dt$ is the material velocity derivative, and ρ is the density of the fluid.

It is also assumed that the materials under study obey the Bingham constitutive equation,

$$\left.\begin{aligned} \underline{\underline{\dot{\gamma}}} &= \underline{\underline{0}}, & \tau < \tau_0 \\ \underline{\underline{\tau}} &= \left(\tfrac{\tau_0}{\dot{\gamma}} + \mu\right)\underline{\underline{\dot{\gamma}}}, & \tau \geq \tau_0 \end{aligned}\right\} \tag{3}$$

where μ is the plastic viscosity, τ_0 is the yield stress of the material,

$$\underline{\underline{\dot{\gamma}}} \equiv \nabla\underline{u} + (\nabla\underline{u})^T \tag{4}$$

is the rate of strain tensor, and the superscript T denotes the transpose. The magnitudes of $\underline{\underline{\dot{\gamma}}}$ and $\underline{\underline{\tau}}$, denoted respectively by $\dot{\gamma}$ and τ, are defined by

$$\dot{\gamma} \equiv \sqrt{\frac{1}{2}II_{\dot{\gamma}}} = \sqrt{\frac{1}{2}\underline{\underline{\dot{\gamma}}} : \underline{\underline{\dot{\gamma}}}} \quad \text{and} \quad \tau \equiv \sqrt{\frac{1}{2}II_{\tau}} = \sqrt{\frac{1}{2}\underline{\underline{\tau}} : \underline{\underline{\tau}}} \tag{5}$$

where the symbol II stands for the second invariant of a tensor. In order to overcome the inherent singularity exhibited by the discontinuous Bingham plastic constitutive model and the associated implementation difficulties in computational codes, we adopt the regularized version of the constitutive Eq. (3), as proposed by Papanastasiou [2,23]:

$$\underline{\underline{\tau}} = \left\{\frac{\tau_o[1-\exp(-m\dot{\gamma})]}{\dot{\gamma}} + \mu\right\}\underline{\underline{\dot{\gamma}}} \tag{6}$$

where m is the stress growth parameter. Eq. (6) is valid uniformly at all levels of $\dot{\gamma}$ and provides a satisfactory approximation of the Bingham plastic model for sufficiently large values of m [16,19,24]. It should be noted, however, that the value of m must be chosen very carefully, since very large values might lead to convergence difficulties [3,12,25].

2.1. The thixotropic model

To characterize the time-dependent flow behavior of the thixotropic, non-linear visco-plastic material and to capture its internal structure evolution during flow, we employ a structural parameter model, which has been extensively used in previous works on semi-solid slurries. A structural parameter, λ, which is a function of time, characterizes the state of the material structure, being unity for fully developed skeleton structure and zero for completely broken structure [3,5,24,26]. The material parameters of the Bingham plastic model, i.e. the plastic viscosity and the yield stress are, in general, functions of λ [24]. In the present work, we assume that the plastic viscosity is constant and that the yield stress in Eq. (3) or its regularized version in Eq. (6) varies as follows:

$$\tau_0(t) = \tau_y\lambda(t) \tag{7}$$

where τ_y is the yield stress of the fully-structured slurry. This simple approach was selected instead of the more complex functional relationship presented by Burgos et al. [24], since the interest here is the very fast structure breakdown associated with the compression test. The evolution of the structural parameter is assumed to follow the first-order rate equation:

$$\frac{D\lambda}{Dt} = a'(1-\lambda) - b'\lambda\dot{\gamma}e^{c'\dot{\gamma}} \tag{8}$$

where a' is the recovery parameter and b' and c' are the breakdown parameters determined from experimental data. The two terms in the RHS of Eq. (8) describe the rates of structure build-up and break-down. The exponential in the second term accounts for the fact that the shear stress evolution in shear rate step-up experiments is typically faster than in the step-down one. This is in line with the experimental data of Modigell and Koke [5,27] on semi-solid slurries, where a strong dependence of the yield stress on the microstructure and the degree of agglomeration of the solid phase was observed, which is further strengthened with rest time. At steady-state the shear rate is constant and the rates of break-down and build-up are equal. One can then determine the equilibrium value of λ:

$$\lambda_e = \frac{1}{1 + (b'/a')\dot{\gamma}_e e^{c'\dot{\gamma}_e}} \tag{9}$$

2.2. Dimensionless equations

To non-dimensionalize the constitutive and the governing equations in the case of squeeze flow under constant velocity U, we scale the lengths by the initial height H_0, the velocity U, the time by H_0/U, and the pressure p and the stresses by the yield stress $\mu U/H_0$. By means of these scalings, the dimensionless forms of Eqs 1, 2, and 6 are as follows:

$$\nabla \cdot \underline{u} = 0 \tag{10}$$

$$Re\frac{D\underline{u}}{Dt} = -\nabla p + \nabla \cdot \underline{\underline{\tau}} \tag{11}$$

and

$$\underline{\underline{\tau}} = \left[Bn\lambda\frac{1-\exp(-M\dot{\gamma})}{\dot{\gamma}} + 1\right]\underline{\underline{\dot{\gamma}}} \tag{12}$$

where for the sake of simplicity, we keep the same symbols for the dimensionless variables. As a result of the non-dimensionalization, there are three dimensionless numbers, namely the Reynolds number,

$$Re \equiv \frac{\rho U H_0}{\mu} \tag{13}$$

the Bingham number

$$Bn \equiv \frac{\tau_y H_0}{\mu U} \tag{14}$$

and the growth number,

$$M \equiv \frac{mU}{H_0} \tag{15}$$

In the case of squeeze flow under constant load F, the following velocity scale is used:

$$U = \frac{F}{\mu H_0} \tag{16}$$

It is implied that the applied load is such that flow does occur, i.e. $F - \pi\tau_0 R_0^2 > 0$.

The dimensionless form of Eq. (8) is

$$\frac{D\lambda}{Dt} = a(1-\lambda) - b\lambda\dot{\gamma}e^{c\dot{\gamma}} \tag{17}$$

where

$$a \equiv \frac{a'H_0}{U}, \quad b \equiv b', \quad c \equiv \frac{c'H_0}{U} \tag{18}$$

are the dimensionless recovery and breakdown parameters.

The boundary conditions of the flow are shown in Fig. 1. Symmetry boundary conditions are imposed along the axis of symmetry and the velocity is set to zero along the bottom. On the free surface it is assumed that surface tension is zero. When the sample is compressed at constant load in the direction of gravity, i.e. the

dimensionless load is of the form $\boldsymbol{F} = -F\mathbf{e}_z$, the dimensionless boundary condition at the top of the sample is given by

$$\int_s (-p\underline{\underline{I}} + \underline{\underline{\tau}}) \cdot \mathbf{e}_z \, dS = -\mathbf{e}_z \tag{19}$$

where S is the surface of the top side of the sample, and $\underline{\underline{I}}$ is the unit tensor. As for the initial conditions, the velocity is everywhere set to zero at $t = 0$.

3. Numerical method

The flow problem is solved in Lagrangian coordinates and thus the position of the free surface is calculated automatically together with the other unknown fields (free surface nodes move with the fluid velocity). The governing equations are discretized using the mixed-Galerkin finite element method with standard nine-node quadrilateral elements for the velocity and four-node ones for the pressure. The resulting non-linear system of equations is solved using a Newton–Raphson iteration procedure with an error tolerance equal to 10^{-5}. Remeshing is achieved by using a Laplace-type discretization algorithm, i.e. a smooth mesh is constructed to conform to the evolving free surface [16]. Care is taken to construct a finer mesh at critical corners. When free-surface nodes touch a solid boundary (i.e. the surface of a disk) they are treated as non-slip boundary nodes, i.e. as nodes that follow the plate. The flow field variables are reassigned new values based on the old mesh [16,28].

4. Numerical results

As already mentioned, in our numerical simulations it is assumed that an incompressible material is compressed only from the top side while the bottom side remains fixed (Fig. 1). The sample is compressed from rest either under constant load or constant velocity. In the former case, the simulations are carried out up to a time when the flow becomes very slow, i.e. the squeeze rate is reduced significantly and no further significant changes in the sample height and shape are observed. In the case of constant velocity, in which the sample height decreases steadily, the simulation is stopped when h becomes 0.15–0.20, that is when the finite elements are very distorted (especially those adjacent to the free surface). Before any meaningful analysis, the effects of the mesh refinement and the magnitude of the growth exponent M on the numerical results have been investigated. Three different meshes have been used, the characteristics of which are tabulated in Table 1. The numerical results presented in this section have been obtained using Mesh 2 (20×20), which gives converged results without significant differences from those obtained with the more refined Mesh 3 (24×24). As for the growth exponent M, we have considered three different values: 100, 300, and 800. The value of $M = 300$ was found to be sufficiently high so that the regularized Papanastasiou model provides a good approximation for the ideal Bingham model; no significant differences were observed from the results obtained with $M = 800$. As already mentioned, very high values of M are undesirable, since they lead to longer computational times and convergence difficulties [18,25,29,30]. Finally, as far as the time step is concerned, this is chosen after extensive numerical experimentation and is kept constant throughout the simulation.

4.1. Simulations under constant load

We first consider as base flow the thixotropic squeeze flow under constant load with $Re = 1$, $Bn = 1$, $a = 1$, $b = 1$ and $c = 0.01$. For the discussion, we also consider the mean structural parameter $\bar{\lambda}$ of the sample, defined by

Table 1
Characteristics of the meshes used in the simulations.

	Elements	Nodes	Unknowns
Mesh 1 (15×15)	225	961	2148
Mesh 2 (20×20)	400	1681	3763
Mesh 3 (24×24)	576	2401	5379

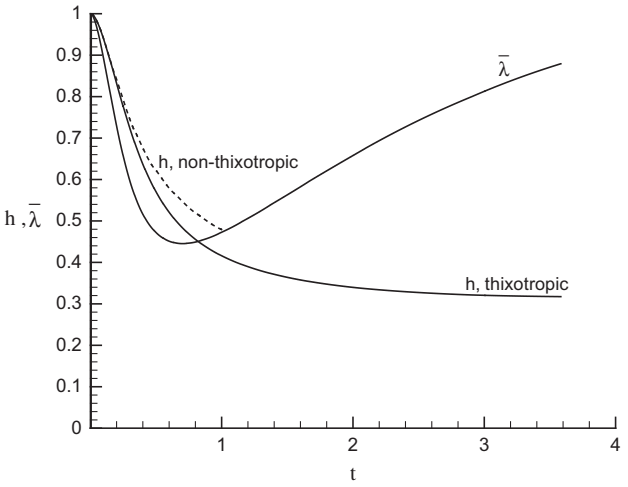

Fig. 2. Evolution of the sample height and the mean structural parameter during squeeze flow under constant load for $Re = 1$, $Bn = 1$, $a = 1$, $b = 1$, and $c = 0.01$. The dashed line is the sample height in the case of a non-thixotropic material ($a = b = c = 0$).

$$\bar{\lambda}(t) \equiv \frac{2\pi}{V_0} \int_0^{h(t)} \int_0^{R(t)} \lambda(r, z, t) r dr dz \tag{20}$$

where V_0 is the total volume of the incompressible sample. The evolution of the sample height and the mean structural parameter are presented in Fig. 2. The sample height decreases monotonically and eventually reaches a plateau, which is, of course, a well-known characteristic of non-thixotropic viscoplastic materials (see, for example, Refs. [16,22]). For comparison purposes the height of a non-thixotropic sample ($a = b = c = 0$) is also plotted. With the inclu-

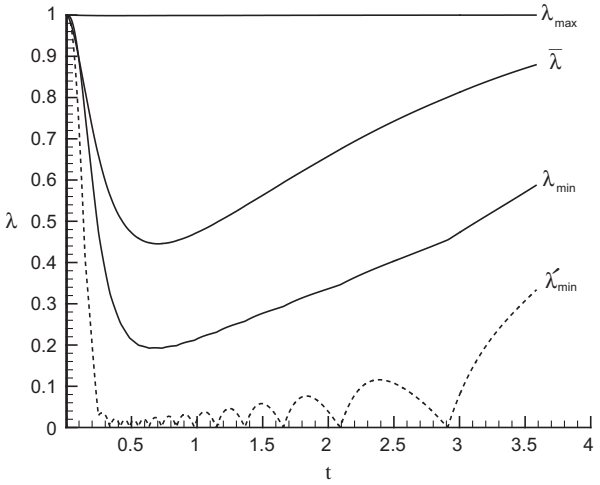

Fig. 3. Evolution of the minimum, maximum and mean structural parameter during squeeze flow under constant load for $Re = 1$, $Bn = 1$, $a = 1$, $b = 1$, and $c = 0.01$. For the calculation of $\lambda_{\min}$ the last two nodes (top of the right edge) have been omitted; the broken line corresponds to the minimum value of $\lambda'_{\min}$ when these two nodes are included.

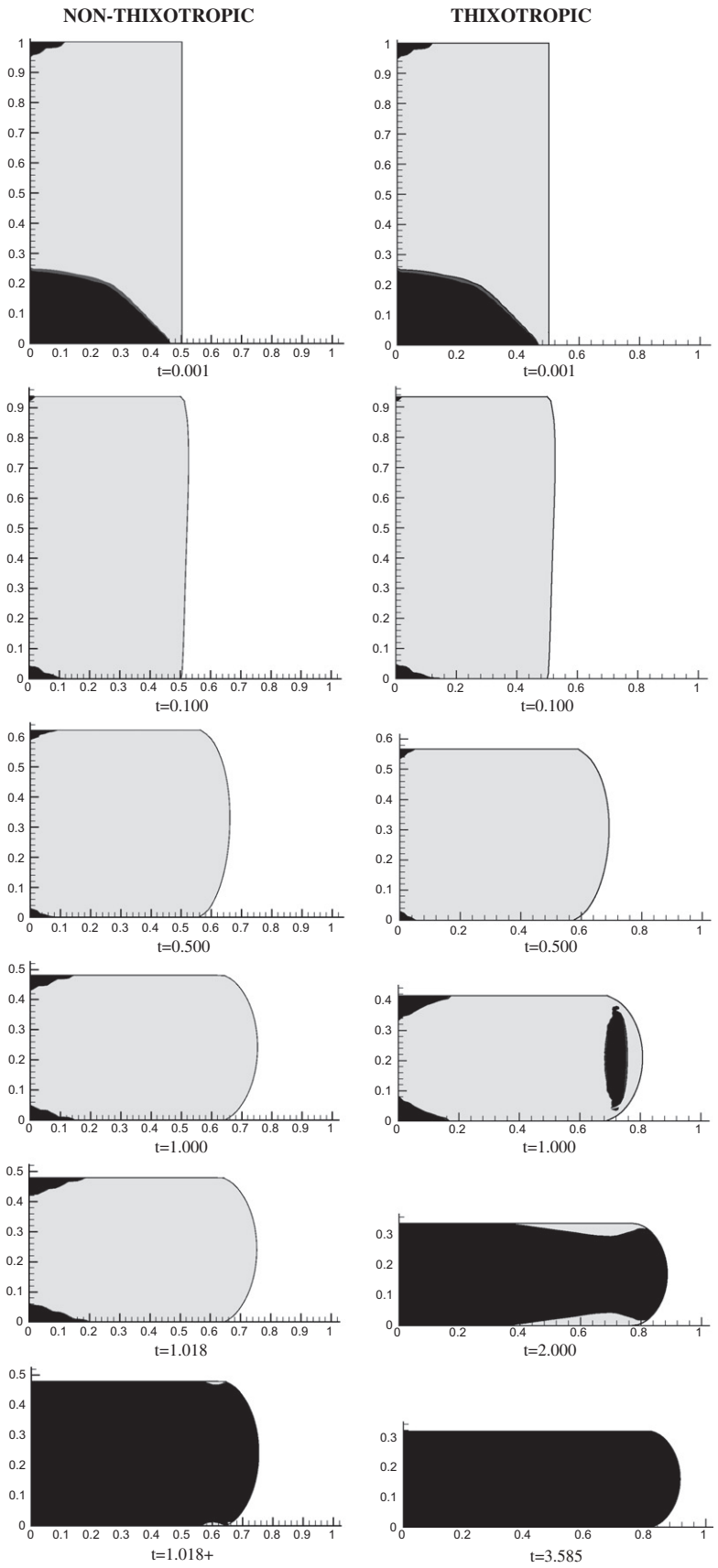

Fig. 4. Yielded (gray) and unyielded (black) areas during squeeze flow of a non-thixotropic (left, $a = b = c = 0$) and a thixotropic material (right, $a = 1$, $b = 1$, $c = 0.01$) under constant load; $Re = 1$, $Bn = 1$.

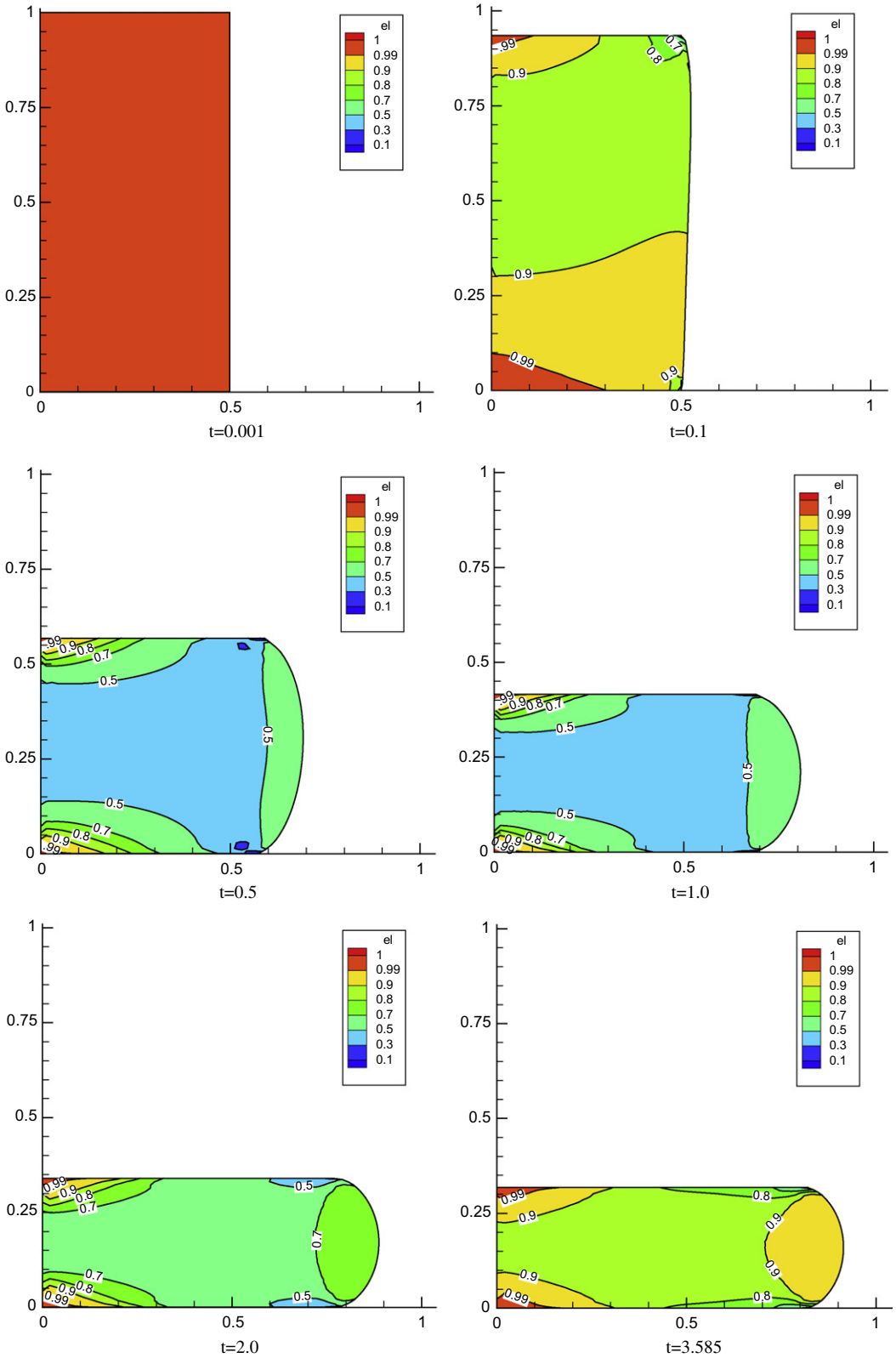

Fig. 5. Contours of the structural parameter λ during squeeze flow under constant load; $Re = 1$, $Bn = 1$, $a = 1$, $b = 1$, and $c = 0.01$.

sion of the structural parameter the duration of the squeeze flow experiment increases and the final sample height is reduced. This is due to the fact that the structure breaks down, resulting in reduced yield stress. This result is consistent with the squeeze flow results of Shaukat et al. [22] on aqueous Laponite suspensions which showed that the final gap height increases with an increase in age of the material as well as with a decrease in the applied force. The mean structural parameter, $\overline{\lambda}$ initially decreases reaching a minimum before the leveling of the sample height, after which build-up is observed. The evolution of λ is shown in Fig. 3, where the

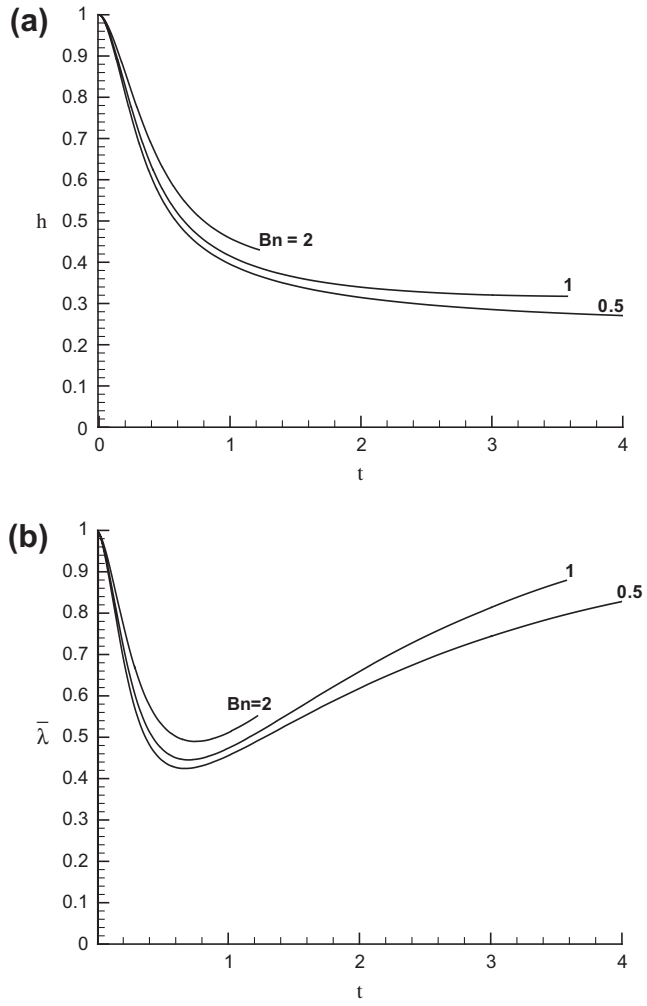

Fig. 6. Effect of the Bingham number on the evolution of (a) the sample height and (b) the mean structural parameter $\bar{\lambda}$; $Re = 1$, $a = 1$, $b = 1$, and $c = 0.01$.

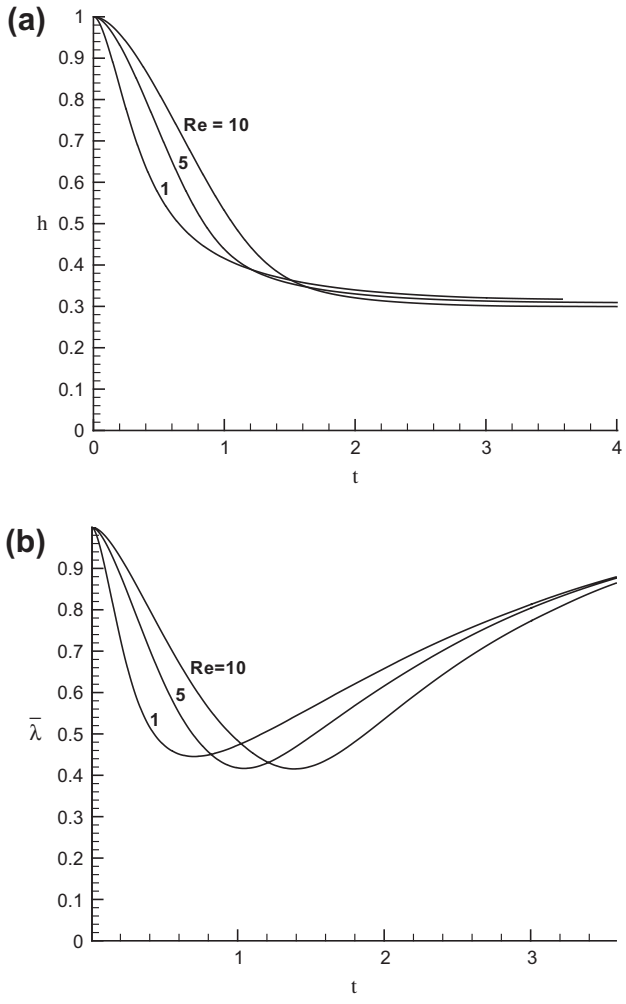

Fig. 7. Effect of the Reynolds number on the evolution of (a) the sample height and (b) the mean structural parameter $\bar{\lambda}$; $Bn = 1$, $a = 1$, $b = 1$, and $c = 0.01$.

maximum and minimum values are also plotted. It seems that λ_{max} is close to unity ($\lambda_{max} > 0.99$), which means that there are always regions where structure is preserved. The behavior of λ_{min} is similar to that of $\bar{\lambda}$. Note that in our base flow no regions with completely broken structure ($\lambda = 0$) are observed. A minimum of about 0.2 is reached at $t \approx 0.5$ and then structure builds up again. It should also be noted that for the calculation of λ_{min} the last 2 nodes at the right upper corner of the sample have been omitted, because they are associated with artificial oscillations of λ (see Fig. 3), as at this place the structure break-down appears to be more intense. These oscillations are due to unavoidable numerical singularities introduced locally due to remeshing and have no significant influence on the global solution.

In Fig. 4 we compare representative snapshots of the yielded (gray) and unyielded (black) regions of our thixotropic base flow to those of its non-thixotropic counterpart ($a = b = c = 0$), obtained under constant load. In the case of non-thixotropic flow, the unyielded regions appear around the axis of symmetry at both the top and bottom of the sample, with the one at the bottom being initially much larger. Both unyielded regions reduce in size as the experiment proceeds. Above a critical time ($t \approx 0.5$), these regions become almost symmetric and then start expanding up to a point that almost the entire material behaves as a rigid solid (at $t = 1.018$). This behavior agrees with previous results for the non-thixotropic flow [16]. Similarly, in the thixotropic case, unyielded regions are initially observed at the top and the bottom of the sample around the axis of symmetry with the latter being larger than the former. It should be noted that in the thixotropic case the unyielded regions are determined based on the local yield stress, i.e. on $Bn_0 = Bn\,\lambda(t)$. As the squeeze flow proceeds, both unyielded regions initially reduce in size and thereafter increase in size again. Eventually they merge to cover almost the entire sample area. The behavior of the thixotropic material may be similar initially, but it gradually becomes quite different. After the initial stage of the experiment, the unyielded regions of the thixotropic material grow in size and eventually a higher squeeze rate is achieved. In addition to the unyielded regions at the top and bottom sides of the sample around the axis of symmetry, a third one appears in the middle of the outer area, which grows and merges with the other two. Apparently, with thixotropy taken into account the build-up phase in the end of the experiment is prolonged so that the sample is compressed more and the unyielded region grows more slowly, allowing the observation of more interesting patterns.

The evolution of the structural parameter is of particular interest in this work. The contours of λ at different times of the squeeze flow experiment are shown in Fig. 5. Initially, the sample is in a fully structured state, i.e. $\lambda = 1$ everywhere. Once the squeeze flow experiment starts, break-down of the inter-particle bonds and structure rearrangement occur at the upper edge of the sample and spread towards the axis of symmetry. As the experiment proceeds, the

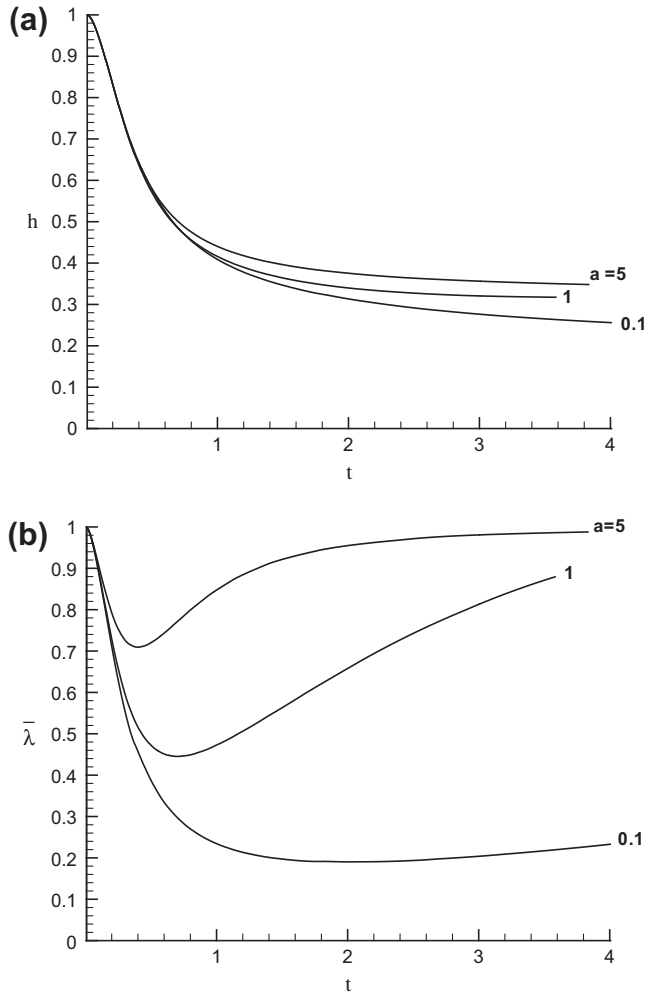

Fig. 8. Effect of the recovery parameter on the evolution of (a) the sample height and (b) the mean structural parameter; $Re = 1$, $Bn = 1$, $b = 1$, and $c = 0.01$.

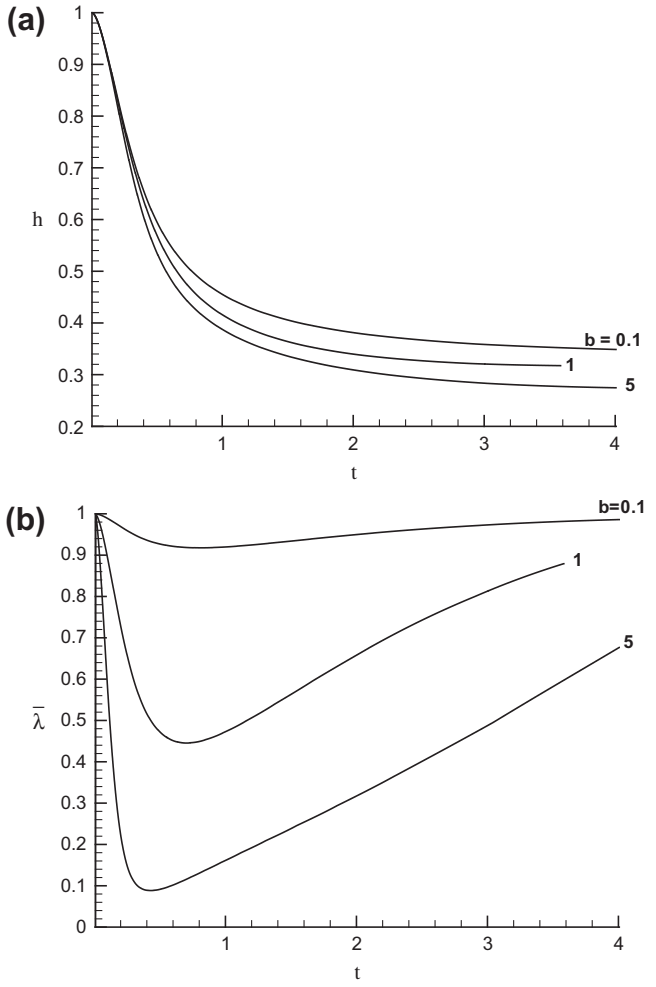

Fig. 9. Effect of the breakdown parameter on the evolution of (a) the sample height and (b) the mean structural parameter; $Re = 1$, $Bn = 1$, $a = 0.1$, and $c = 0.01$.

structure changes everywhere in the sample. The lower values of λ occur at the middle of the sample around the axis of symmetry, and at its top and bottom edges, closer to the outer surface of the sample than to the symmetry axis. Therefore, important phenomena occur in the initial stages of the squeeze flow experiment. However, during squeeze flow, the structural parameter, λ, at the top and the bottom sides of the sample around the axis of symmetry remains close to unity. As also indicated in Fig. 3, after the initial break-down, a build-up is observed and the structural parameter increases everywhere in the sample approaching unity. Comparing Figs. 4b and 5 we observe that the unyielded regions in the sample occur mainly in places where higher values of λ are calculated, i.e. where more particles are welded together. The squeeze flow of the sample fails to proceed at the time where $\lambda > 0.7$ everywhere in the sample and the entire material behaves as a rigid solid. To our knowledge, this is the first time where contours of the structural parameter are provided in the case of a squeeze flow experiment.

The effect of the Bingham number on the height and the mean structural parameter is illustrated in Fig. 6. In agreement with previous works for non-thixotropic yield stress fluids [16,31], the squeeze rate becomes lower and the final sample height increases with the Bingham number. In Fig. 6b, we observe that the breakdown of the welded particles becomes slower at higher Bingham numbers and continues reaching a minimum value after which a build-up occurs [3,12,32]. The resulting minimum is thus higher

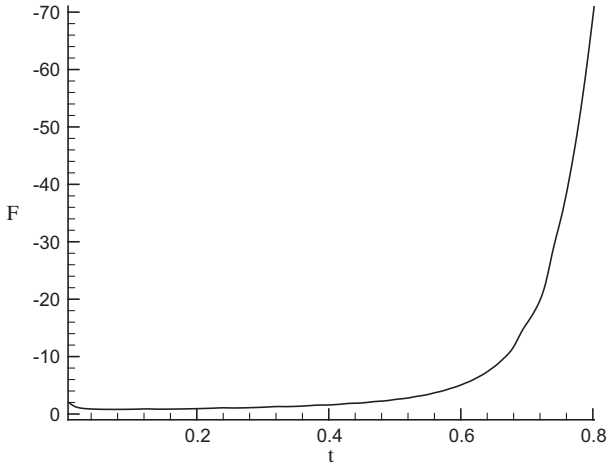

Fig. 10. Effect of the load on the compression under constant velocity; $Re = 1$, $Bn = 1$, $a = 1$, $b = 1$, and $c = 0.01$.

and is shifted to the right. In the build-up stage the material regains its structure faster as Bn increases, due to reduced shearing.

In Fig. 7 we ploted evolution of h and $\bar{\lambda}$, for different Reynolds numbers. The squeeze rate appears to decelerate with the Reynolds

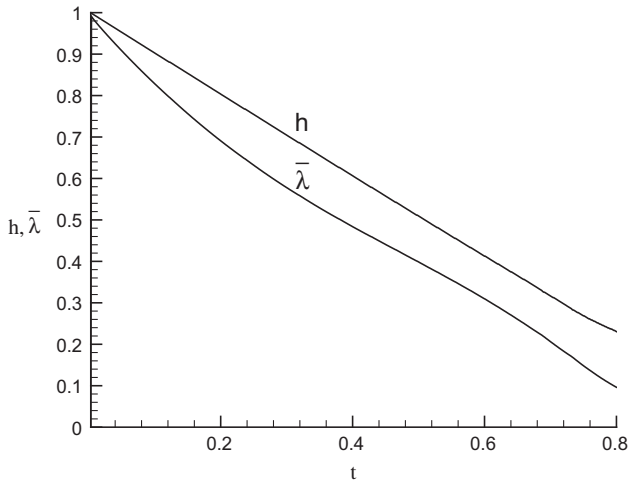

Fig. 11. Evolution of the sample height and the mean structural parameter during squeeze flow under constant velocity; $Re = 1$, $Bn = 1$, $a = 1$, $b = 1$, and $c = 0.01$.

number, which is counter-intuitive. However, this is due to our non-dimensionalization; increasing the Reynolds number is equivalent to increasing the density of the fluid, while all other parameters remain the same [16]. The overlapping of the curves corresponding to different Reynolds numbers is due to the fact that the effective stress field in the sample is eventually reduced below the material's yield stress. The curves of the mean structural parameter show that as the *Re* increases the breakage of the welded particles decelerates and the minimum value of $\bar{\lambda}$ is slightly lowered.

The effects of the recovery and break-down parameters on the squeeze rate and the mean structural parameter of the base flow are illustrated in Figs. 8 and 9, respectively. The squeeze rate appears not to be affected initially by a, but as the experiment proceeds, the flow decelerates at higher values of a with significant reduction on the final height of the compressed sample (Fig. 8). Naturally, the mean structural parameter increases significantly with the recovery parameter, i.e. the effect of build-up due to particle interaction becomes more intensive, causing the material to regain its solid structure faster and $\bar{\lambda}$ to go to unity. For $a = 0.1$, structure build-up is so slow that the experiment stops when $\bar{\lambda}$ is slightly above its minimum value. Obviously, the effect of the break-down parameter b is opposite to that of a. Therefore, as shown in Fig. 9, the rate of squeezing increases with b, i.e. the structure break-down becomes faster. The results for $\bar{\lambda}$ confirm that by increasing b the material bonds are forced to break-up faster with significant reduction of the mean structural parameter. When $b = 5$, $\bar{\lambda}$ is reduced significantly down to 0.1 in a relatively short time and then increases steadily as structure is build-up.

4.2. Simulations under constant velocity

Let us now consider the squeeze flow under constant velocity with $Re = 1$, $Bn = 1$, $a = 1$, $b = 1$, and $c = 0.01$. The required load for compressing the material is plotted in Fig. 10. Initially the load is very high and decreases rapidly reaching a minimum after which a progressive increase occurs. Later, as the sample top surface expands, the load increases exponentially. As already mentioned, at a certain critical time the simulation is stopped, due to excessive distortion of the finite elements (the sample becomes very thin). It should be noted that a smoothing of the load curve has been employed, in order to eliminate artificial spikes in the pressure (and hence in the calculation of the load) due to the discrete advancing of the nodal points on the solid surface. The plots of the sample height and the mean structural parameter are given in Fig. 11. In contrast to the flow under constant load, the mean structural parameter is reduced monotonically reaching a final value of 0.1, which implies that in squeeze flow the structure is destroyed steadily.

The evolution of the yielded (gray) and unyielded (black) regions is illustrated in Fig. 12. An unyielded region is observed initially at the bottom of the sample around the axis of symmetry. This appears to somehow increase in size and then to decrease. Later on an unyielded region appears at the top side of the sample (around the axis of symmetry). As the squeeze flow proceeds both unyielded areas decrease in size and they finally disappear. The evolution of the structural parameter contours during squeeze flow under constant velocity is illustrated in Fig. 13. As with the experiment under constant load (Fig. 5) the break-down of the inter-particle bonds begins with the squeeze flow initialization, starting from the upper edge of the sample and spreading towards the axis of symmetry. The average broken bonds and particle rearrangement increase along the whole material with the value of $\lambda < 0.1$ occurring at the top and the bottom edges near the outer surface. At the top and bottom sides of the sample around the axis of symmetry λ increases steadily approaching unity. As already mentioned, no build-up of the material structure is observed in contrast to the constant load experiment.

The effects of the recovery and the break-down parameters on the resulting load and the mean structural parameter are illustrated in Figs. 14 and 15, respectively. The necessary load for compressing the sample under constant velocity increases very slightly with the recovery parameter. It is clear that break-down occurs faster for lower values of a and the entire phenomenon is irreversible (Fig. 14), while the resulting load decreases for higher values of the break-down parameter (Fig. 15a). As expected, the structural parameter decreases significantly at higher values of b (Fig. 15b), a phenomenon which appears to be also irreversible. Obviously, the reduction of $\bar{\lambda}$ for $b = 5$ occurs in a relatively short time leading to a value lower than 0.1.

The present simulations show clearly that the results from the squeeze flow experiment can vary and they depend on whether the sample is squeezed under constant force or under constant velocity. These differences, of course, cannot be seen when thixotropy is not accounted for. As the slurries are indeed thixotropic, it is important to exploit these differences by isolating the effects of built up and breakdown. When the sample is squeezed under constant velocity the average rate of strain is fixed by the velocity. The average strain everywhere within the sample increases with increasing compression. Hence, during compression the structure everywhere within the sample breaks down continuously. Therefore, except for extreme values of the recovery parameter, the structure is destroyed in relatively short times and the rate of buildup is not important. Possible unyielded regions within the sample disappear in a very short time. When, however, the sample is squeezed under constant force the situation is very different. During compression as the sample is squeezed the compressed area increases. Therefore the imposed stress on the sample decreases. The flow and topography of the yielded and unyielded regions result from a competition between the local stress, the rate of strain and both, the breakdown and recovery parameters. Both the flow field and the unyielded regions are more complex than the case of compression under constant velocity. These differences and the complexity of the resulting flow field show clearly that the only way to extract reliable data is by using computational rheology and reverse engineering.

5. Concluding remarks

A thixotropic model based on the Bingham plastic constitutive equation with the yield stress linearly dependent on a structural

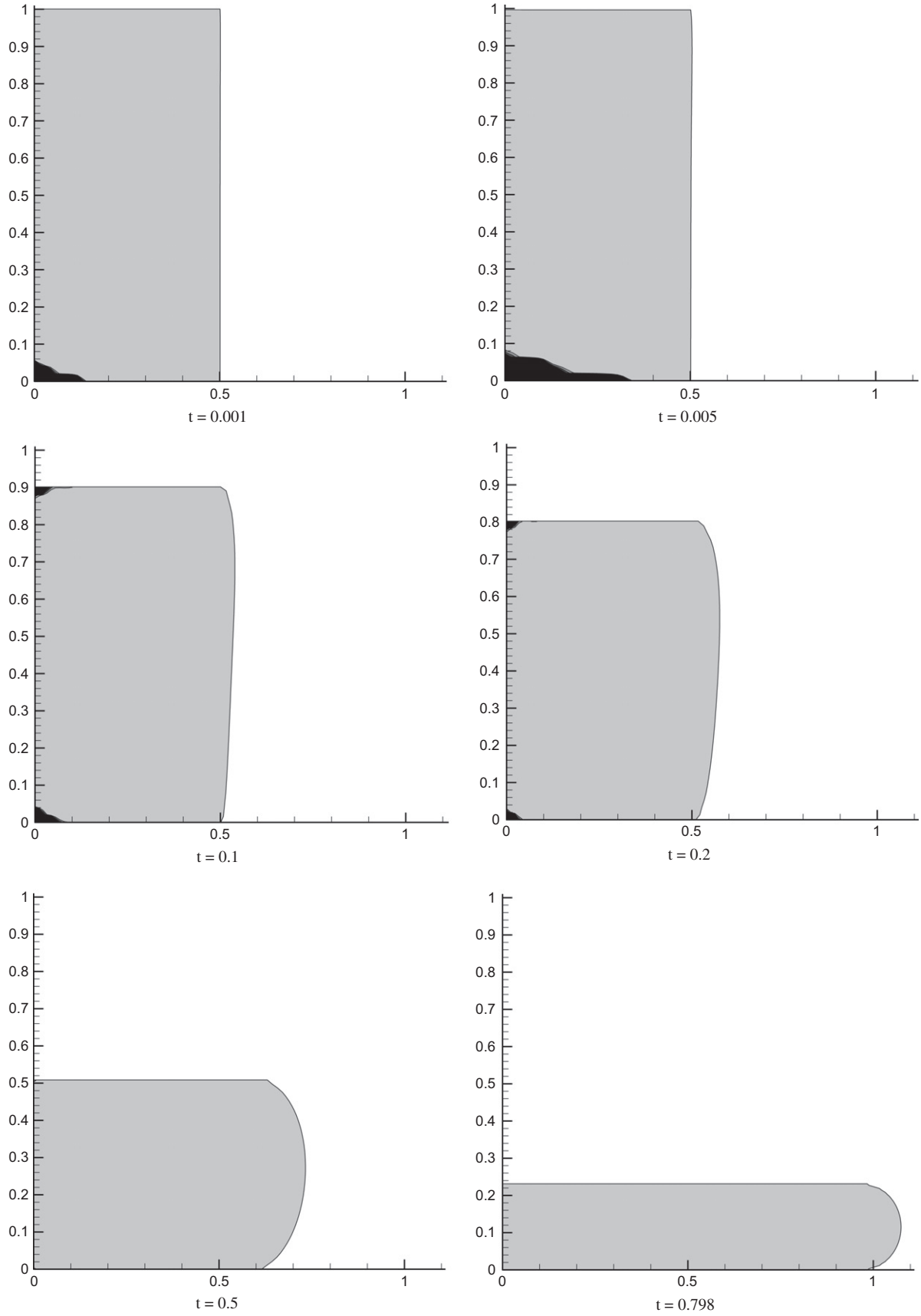

Fig. 12. Evolution of the yielded (gray) and unyielded (black) areas during squeeze flow simulation under constant velocity; $Re = 1$, $Bn = 1$, $a = 1$, $b = 1$, and $c = 0.01$.

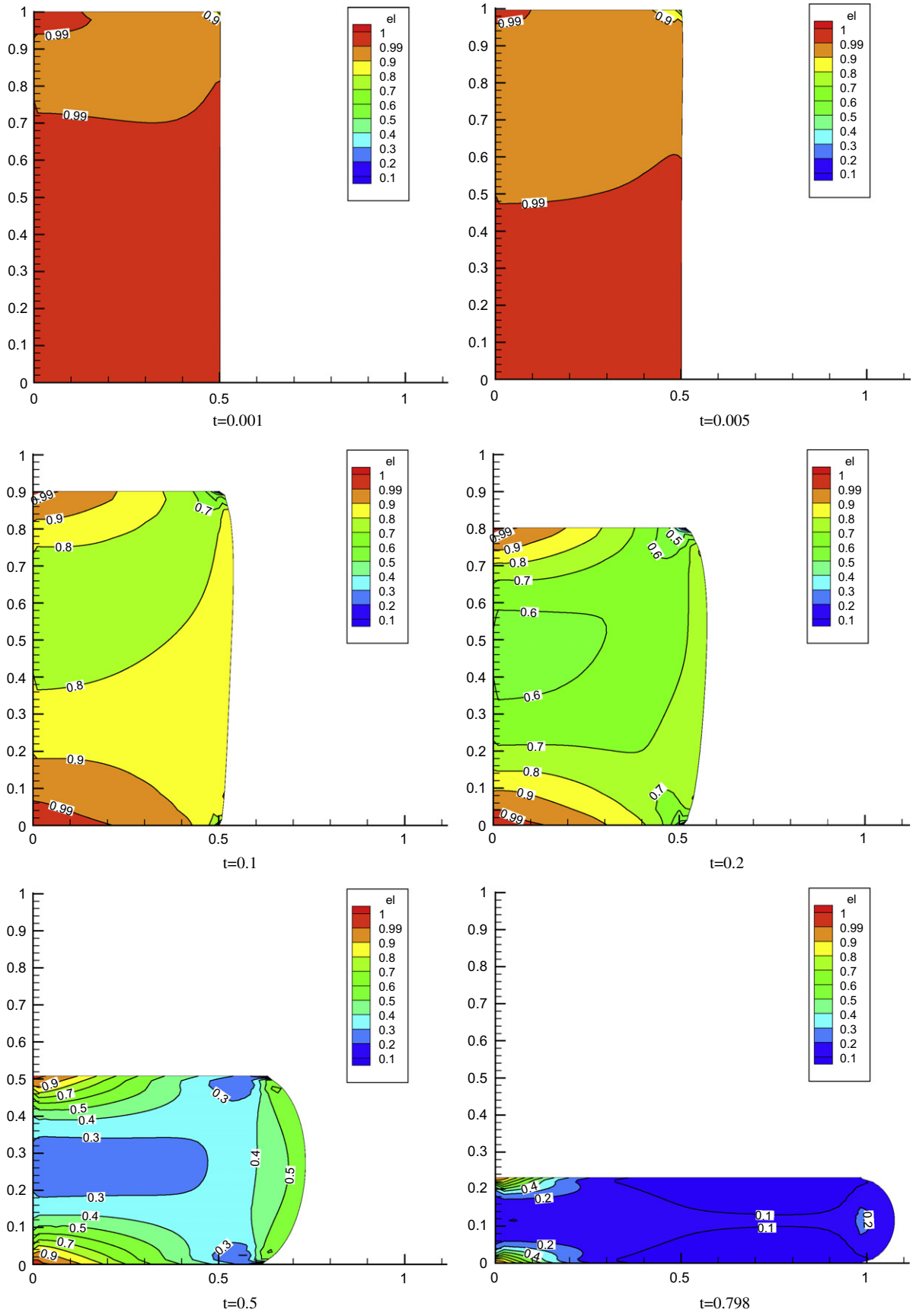

Fig. 13. Contours of the structural parameter λ during squeeze flow simulation under constant velocity; $Re = 1$, $Bn = 1$, $a = 1$, $b = 1$, and $c = 0.01$.

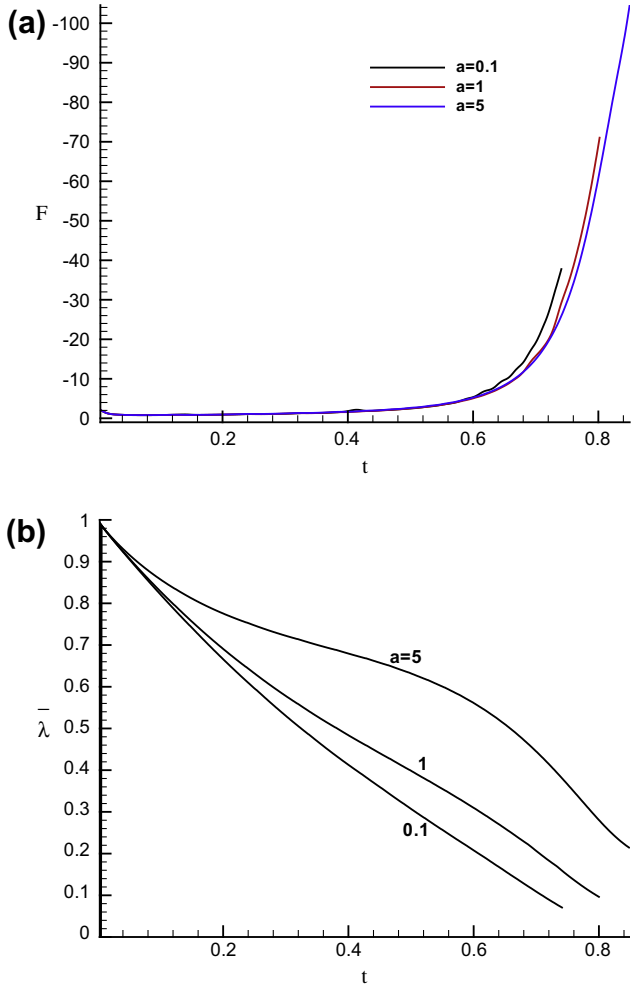

Fig. 14. Effect of the recovery parameter on the evolution of (a) the sample height and (b) the mean structural parameter during squeeze flow under constant velocity; $Re = 1$, $Bn = 1$, $b = 1$, and $c = 0.01$.

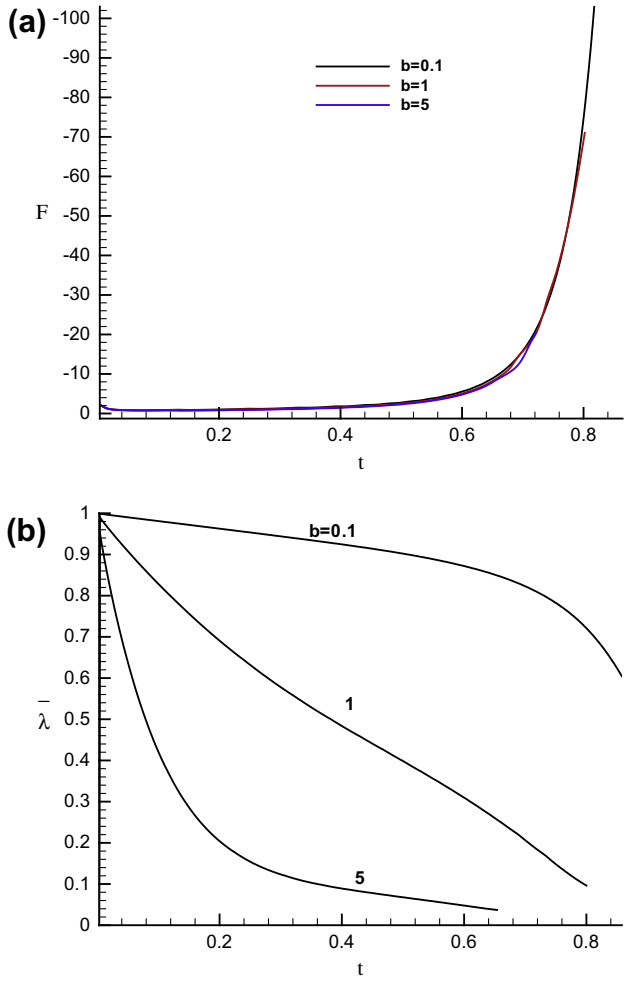

Fig. 15. Effect of the breakdown parameter on the evolution of (a) the sample height and (b) the mean structural parameter during squeeze flow under constant velocity; $Re = 1$, $Bn = 1$, $a = 0.1$, and $c = 0.01$.

parameter has been employed in order to study the flow behavior of a thixotropic, viscoplastic material and the evolution of its structural state during squeeze flow either under constant load or constant velocity. A first-order rate equation was used to describe the evolution of the internal structure of the sample.

Two-dimensional results for the evolution of the structural parameter have been presented for the first time and compared to the evolution of the corresponding yielded and unyielded regions. In the case of squeeze flow under constant load, the average value of the structural parameter, $\bar{\lambda}$, appears to decrease initially reaching a minimum, after which build-up is observed. The maximum value of the structural parameter in the sample remains close to unity ($\lambda_{max} > 0.99$), which means that there are always regions where structure is preserved. This is not the case in squeeze flow under constant velocity, where $\bar{\lambda}$ decreases monotonically down to values as low as 0.1, which indicates that structure is almost broken everywhere in the sample. During the initial stage of the compression, thixotropy does not affect the flow. However, as the experiment proceeds, a higher rate of compression and a slower growth of the unyielded regions are observed for the thixotropic material.

The present numerical simulations are encouraging as they could contribute to the development of a methodology for the determination of the material constants of semi-solid slurries used in the processing of alloys, which behaves as thixotropic, non-linear visco-plastic material with history-dependent material-parameters. Evidently, further investigation of the time-dependent behavior of thixotropic materials and the internal structural evolution is needed for achieving this objective.

It will be interesting to employ the present model in simulating squeeze flow experiments in which the sample is squeezed down to a given height and then is left at rest for a specified time after which compression continues. Such experiments have been carried out by Rodts et al. [33] on bentonite suspensions; they reported that starting from different times of rest the material undergoes similar changes in structure and only the force is reduced.

Acknowledgements

We would like to thank the two anonymous reviewers for their comments and suggestions which have been very helpful.

References

[1] M.C. Flemings, Behaviour of metal alloys in the semisolid state, Metall. Trans. A22 (1991) 957–981.
[2] A.N. Alexandrou, Y. Pan, D. Apelian, G. Georgiou, Semisolid material characterization using computational rheology, in: Y. Tsutsui, M. Kiuchi, K. Ichikawa (Eds.), Proceedings of the 7th International Conference on Semi-Solid Processing of Alloys and Composites, Tsukuba, Japan, 2002, pp. 417–422.

[3] A.N. Alexandrou, N. Constantinou, G. Georgiou, Shear rejuvenation, aging and shear banding in yield stress fluids, J. Non-Newtonian Fluid Mech. 158 (2009) 6–17.
[4] V. Favier, H. Atkinson, Analysis of semi-solid response under rapid compression test using multi-scale modelling and experiments, Trans. Nonferrous Met. Soc. China 20 (2010) 1691–1695.
[5] M. Modigell, J. Koke, Time-depended rheological properties of semisolid metal alloys, Mech. Time-Dependent Mater. 3 (1999) 15–30.
[6] L. Azzi, F. Ajersch, Analytical modelling of the rheological behavior of semisolid metals and composites, Metall. Mater. Trans. B 37 (2006) 1067–1074.
[7] J. Mewis, N.J. Wagner, Thixotropy, Adv. Colloid Interface Sci. 147–148 (2009) 214–227.
[8] J. Mewis, Thixotropy – a general review, J. Non-Newtonian Fluid Mech. 6 (1979) 1–20.
[9] H.A. Barnes, Thixotropy – a review, J. Non-Newtonian Fluid Mech. 70 (1997) 1–33.
[10] A. Mujumdar, A.N. Beris, A.B. Metzner, Transient phenomena in thixotropic systems, J. Non-Newtonian Fluid Mech. 102 (2002) 157–178.
[11] P.R. de Souza Mendes, Modeling the thixotropic behavior of structured fluids, J. Non-Newtonian Fluid Mech. 164 (2009) 66–75.
[12] A.N. Alexandrou, G. Georgiou, On the early breakdown of semisolid suspensions, J. Non-Newtonian Fluid Mech. 142 (2007) 199–206.
[13] A.N. Beris, E. Stiakakis, D. Vlassopoulos, A thermodynamically consistent model for thixotropic behavior of concentrated star polymer suspensions, J. Non-Newtonian Fluid Mech. 152 (2008) 76–85.
[14] B.P. Gautham, P.C. Kapur, Rheological model for short duration response of semi-solid metals, Mater. Sci. Eng. A393 (2005) 223–228.
[15] R. Koeune, J.-P. Ponthot, An improved constitutive model for the numerical simulation of semi-solid thixoforming, J. Comput. Appl. Math. 234 (2010) 2287–2296.
[16] G.C. Florides, A.N. Alexandrou, G. Georgiou, Flow development in compression of a finite amount of a Bingham plastic, J. Non-Newtonian Fluid Mech. 143 (2007) 38–47.
[17] A. Potanin, 3D simulation of the flow of thixotropic fluids, in large-gap Couette and vane-cup geometries, J. Non-Newtonian Fluid Mech. 165 (2010) 299–312.
[18] H.A. Ardakani, E. Mitsoulis, S.G. Hatzikiriakos, Thixotropic flow of toothpaste through extrusion dies, J. Non-Newtonian Fluid Mech. 166 (2011) 1262–1271.
[19] D.N. Smyrnaios, J.A. Tsamopoulos, Squeeze flow of Bingham plastics, J. Non-Newtonian Fluid Mech. 100 (2001) 165–190.
[20] J. Engmann, C. Serrais, A.S. Burbidge, Squeeze flow theory and applications to rheometry: a review, J. Non-Newtonian Fluid Mech. 132 (2005) 1–27.
[21] N. Roussel, C. Lanos, Z. Toutou, Indentification of Bingham fluid flow parameters using a simple squeeze test, J. Non-Newtonian Fluid Mech. 135 (2006) 1–7.
[22] A. Shaukat, A. Sharma, Y.M. Joshi, Squeeze flow behavior of (soft glassy) thixotropic material, J. Non-Newtonian Fluid Mech. 167–168 (2012) 9–17.
[23] T.C. Papanastasiou, Flows of materials with yield, J. Rheol. 31 (1987) 385–404.
[24] G.R. Burgos, A.N. Alexandrou, V.M. Entov, Thixotropic behavior of semisolid slurries, J. Mater. Process. Technol. 110 (2001) 164–176.
[25] K.R.J. Ellwood, G.C. Georgiou, T.C. Papanastasiou, J.O. Wilkes, Laminar jets of Bingham-plastic liquids, J. Rheol. 34 (1990) 787–812.
[26] P. Kumar, C.L. Martin, S. Brown, Constitutive modeling and characterization of the flow behavior of semi-solid metal alloy slurries. I. The flow response, Acta Metall. Mater. 42 (11) (1994) 3595–3602.
[27] J. Koke, M. Modigell, Flow behavior of semi-solid metal alloys, J. Non-Newtonian Fluid Mech. 112 (2003) 141–160.
[28] G.R. Burgos, Rheology of Semisolid Metal Suspensions, PhD Thesis, Worchester Polytechnic Institute, 1999.
[29] A.N. Alexandrou, T.M. McGilvreay, G. Burgos, Steady Herschel–Bulkley fluid flow in three dimensional expansions, J. Non-Newtonian Fluid Mech. 100 (2001) 77–96.
[30] I.A. Frigaard, C. Nouar, On the usage of viscosity regularization methods for visco-plastic fluid flow computation, J. Non-Newtonian Fluid Mech. 127 (2005) 1–26.
[31] G. Karapetsas, J. Tsamopoulos, Transient squeeze flow of viscoplastic materials, J. Non-Newtonian Fluid Mech. 133 (2006) 35–56.
[32] G.R. Burgos, A.N. Alexandrou, V.M. Entov, On the determination of yield surfaces in Herschel–Bulkley fluids, J. Rheol. 43 (1999) 463–483.
[33] S. Rodts, J. Boujlel, B. Rabideau, G. Ovarlez, N. Roussel, P. Moucheront, C. Lanos, F. Bertrand, P. Coussot, Solid–liquid transition and rejuvenation similarities in complex flows of thixotropic materials studied by NMR and MRI, Phys. Rev. E 81 (2010) 021402.